Bonn-TH-2012-19
IFIC/12-57
CFTP/12-012

A novel way of constraining WIMPs annihilations in the Sun: MeV neutrinos

Nicolás Bernal[1], Justo Martín-Albo[2] and Sergio Palomares-Ruiz[3]

[1]*Bethe Center for Theoretical Physics and Physikalisches Institut, Universität Bonn, Nußallee 12, D-53115 Bonn, Germany*

[2]*Instituto de Física Corpuscular (IFIC), CSIC-Universitat de València, Apartado de Correos 22085, E-46071 Valencia, Spain and*

[3]*Centro de Física Teórica de Partículas (CFTP), Instituto Superior Técnico, Universidade Técnica de Lisboa, Av. Rovisco Pais 1, 1049-001 Lisboa, Portugal*

Abstract

Annihilation of dark matter particles accumulated in the Sun would produce a flux of high-energy neutrinos whose prospects of detection in neutrino telescopes and detectors have been extensively discussed in the literature. However, for annihilations into Standard Model particles, there would also be a flux of neutrinos in the MeV range from the decays at rest of muons and positively charged pions. These low-energy neutrinos have never been considered before and they open the possibility to also constrain dark matter annihilation in the Sun into e^+e^-, $\mu^+\mu^-$ or light quarks. Here we perform a detailed analysis using the recent Super-Kamiokande data in the few tens of MeV range to set limits on the WIMP-nucleon scattering cross section for different annihilation channels and computing the evaporation rate of WIMPs from the Sun for all values of the scattering cross section in a consistent way.

I. INTRODUCTION

There is overwhelming evidence of the existence of a massive non-baryonic dark component which contributes to about 80% of the energy budget of the Universe [1–5], being a weakly interacting massive particle (WIMP), with mass lying from the GeV to the TeV scale, one of the most popular candidates.

One of the different proposed strategies to detect WIMPs is to search for the flux of high-energy neutrinos from the annihilations of WIMPs accumulated in the center of the Sun [6–9]. Many different studies have evaluated the prospects of detection of these neutrinos with neutrino telescopes/detectors [10–20]. However, previous works have focused on WIMPs annihilations into hadronic or $\tau^+\tau^-$ channels. On the other hand, annihilations into $\mu^+\mu^-$ or light quarks have always been neglected, for muons and pions lose energy very effectively in the dense regions where they would be produced and then would decay at rest, giving rise to neutrinos in the MeV range. Likewise, annihilations into e^+e^- have never been considered, for they would not produce directly neutrinos. Nevertheless, in their propagation through the Sun they would interact with nuclei and produce pions, which would be stopped. The π^- would then get captured and subsequently absorbed by the nuclei of the medium, but the π^+ would decay at rest, producing a flux of MeV neutrinos. On the other hand, hadronic and $\tau^+\tau^-$ channels, along with heavy mesons (the source of the high-energy neutrinos considered so far), would also produce light mesons, as pions, which would then be stopped and (in the case of π^+) decay at rest. The energies of these neutrinos lie at the energy range where the diffuse supernova neutrino background (DSNB) is searched for by detectors such as Super-Kamiokande (SK) [21, 22][1].

Here we consider, for the first time[2], the potential signal of these low-energy neutrinos from WIMPs annihilations in the Sun and use the most recent SK data [21, 22], and analogously to the SK collaboration, we perform an extended maximum likelihood analysis in order to set bounds on the scattering cross section of WIMPs off nucleons for different annihilation channels. In this work we calculate the evaporation rate of WIMPs from the Sun for

[1] It is interesting to note that this is also the energy region for GUT monopole searches at SK [23], which have a spectral signal of the same type of the one discussed in this work. However, in that analysis only angular bins were considered, whereas in this work we make use of the full energy spectrum.

[2] This idea was simultaneously proposed by Ref. [24]. Both works were made publicly available on the arXiv the very same day.

all values of the scattering cross section in a consistent way and note that in the optically thick regime, it *decreases* with the cross section, which allows us to set limits to WIMP masses usually not considered within this context.

II. CAPTURE, ANNIHILATION AND EVAPORATION OF WIMPS IN THE SUN

Galactic WIMPs would get eventually trapped in the Sun if, after many elastic scatterings off the solar nuclei, they lose energy and their velocity gets lower than the Sun's escape velocity. If the mean free path of WIMPs is large compared to the size of the Sun (the Knudsen limit or optically thin regime), they would thermalize non-locally by multiple interactions, so their density could be approximated as an isothermal sphere following the law of atmospheres, with a radial dependence set by the gravitational potential [25, 26]

$$n_{\chi(r),\mathrm{iso}}(r,t) = N_\chi(t)\,\frac{e^{-m_\chi\phi(r)/T_\chi}}{\int_0^{R_\odot} 4\pi r^2 dr\, e^{-m_\chi\phi(r)/T_\chi}}\ , \tag{1}$$

where $N_\chi(t)$ is the total population of WIMPs with mass m_χ, $\phi(r) = \int_0^r GM_\odot(r')/r'^2 dr'$ the solar gravitational potential at r and T_χ the average WIMPs temperature, calculated by imposing that there is no net flow of energy [25] and using the Standard Solar Model (SSM) [27, 28] (we consider 29 elements).

However, for large cross sections (optically thick regime), WIMPs would be in local thermal equilibrium and their density distribution could be approximated as [29, 30]

$$n_{\chi(r),\mathrm{LTE}}(r,t) = n_{\chi,\mathrm{LTE}}(0,t)\,\left(\frac{T_\odot(r)}{T_\odot(0)}\right)^{3/2}\exp\left(-\int_0^r \frac{\alpha(r')\frac{dT_\odot(r',t)}{dr'} + m_\chi\frac{d\phi(r')}{dr'}}{T_\odot(r')}dr'\right)\ , \tag{2}$$

where $T_\odot(r)$ is the solar temperature at radius r and $n_{\chi,\mathrm{LTE}}(0,t)$ is set by the normalization $\int_0^{R_\odot} 4\pi r^2 dr\, n_{\chi,\mathrm{LTE}}(r,t) = N_\chi(t)$. The factor $\alpha(r)$ is the dimensionless thermal diffusivity and, for a given admixture of elements in the medium, a good approximation is to take the weighted mean of the solutions to the single-element case [30, 31],

$$\alpha(r) = \ell(r)\sum_i \ell_i(r)^{-1}\,\alpha_0(m_i/m_\chi)\ , \tag{3}$$

where α_0 is the diffusivity for one element and is tabulated as a function of m_i/m_χ in Ref. [30], where m_i is the mass of the i-th nuclear species. The quantity $\ell(r) = (\sum_i \ell_i(r)^{-1})^{-1}$ is the total mean free path of WIMPs and $\ell_i(r) = (\sigma_i n_i(r))^{-1}$ is the partial mean free path for

WIMP interactions with cross section σ_i off the i-th nuclear species with density $n_i(r)$, for which we use the SSM [27, 28]. Depending on the type of interactions, either spin-dependent or spin-independent, the cross section is given by

$$\sigma_i^{\rm SD} \;=\; \left(\frac{\mu_i}{\mu_{\rm p}}\right)^2 \frac{4(J_i+1)}{3J_i} \left|\langle S_{{\rm p},i}\rangle + {\rm sign}(a_{\rm p}a_{\rm n}) \left(\frac{\mu_p}{\mu_n}\right) \sqrt{\frac{\sigma_{\rm n}^{\rm SD}}{\sigma_{\rm p}^{\rm SD}}} \langle S_{{\rm n},i}\rangle\right|^2 \sigma_{\rm p}^{\rm SD} \;, \tag{4}$$

$$\sigma_i^{\rm SI} \;=\; \left(\frac{\mu_i}{\mu_p}\right)^2 \left|Z_i + (A_i - Z_i)\,{\rm sign}(f_{\rm p}f_{\rm n}) \left(\frac{\mu_p}{\mu_n}\right) \sqrt{\frac{\sigma_{\rm n}^{\rm SI}}{\sigma_{\rm p}^{\rm SI}}}\right|^2 \sigma_{\rm p}^{\rm SI} \;, \tag{5}$$

where μ_i ($\mu_{p/n}$) is the reduced mass of the WIMP-nucleus i (WIMP-proton/neutron) system, $\sigma_{\rm p}^{\rm SD}$ ($\sigma_{\rm n}^{\rm SD}$) and $\sigma_{\rm p}^{\rm SI}$ ($\sigma_{\rm n}^{\rm SI}$) are the spin-dependent and spin-independent elastic scattering WIMP cross section off protons (neutrons), respectively, Z_i, A_i and J_i are the atomic number, the mass number and the spin of the nucleus i, and $\langle S_{{\rm p},i}\rangle$ and $\langle S_{{\rm n},i}\rangle$ are the expectation values of the spins of protons and neutrons averaged over all nucleons, respectively, which we take from Refs. [32–35]. The quantities $a_{\rm p}$ ($f_{\rm p}$) and $a_{\rm n}$ ($f_{\rm n}$) are the axial (scalar) four-fermion WIMP-nucleon couplings. As usual, we assume $\sigma_{\rm p}^{\rm SD} = \sigma_{\rm n}^{\rm SD}$, $\sigma_{\rm p}^{\rm SI} = \sigma_{\rm n}^{\rm SI} \equiv \sigma^{\rm SI}$ and the same sign for the couplings, so Eqs. (4) and (5) get simplified as

$$\sigma_i^{\rm SD} \;=\; \left(\frac{\mu_i}{\mu_{\rm p}}\right)^2 \frac{4(J_i+1)}{3J_i} \left|\langle S_{{\rm p},i}\rangle + \langle S_{{\rm n},i}\rangle\right|^2 \sigma_{\rm p}^{\rm SD} \;, \tag{6}$$

$$\sigma_i^{\rm SI} \;=\; \left(\frac{\mu_i}{\mu_{\rm p}}\right)^2 A_i^2\,\sigma^{\rm SI} \;. \tag{7}$$

Nevertheless, in the case of spin-dependent cross section it is the coupling with protons which is mainly probed, for almost all WIMPs interactions are off hydrogen.

The transition from one regime to the other is indicated by the so-called Knudsen number,

$$Kn \equiv \frac{\ell(0)}{r_\chi} \;, \tag{8}$$

where $r_\chi = \left(\frac{3\,T(0)}{2\pi G\,\rho(0)\,m_\chi}\right)^{1/2}$ is the approximate scale height of the WIMP distribution, with G the gravitational constant and $\rho(0)$ the density at the solar center. In order to interpolate between the optically thin ($Kn \gg 1$) and the optically thick ($Kn \ll 1$) regimes we follow the approach of Ref. [36], motivated by the results of Ref. [30], and approximate the total WIMP distribution as

$$n_\chi(r,t) \;=\; \mathfrak{f}(Kn)\, n_{\chi,{\rm LTE}}(r,t) + (1-\mathfrak{f}(Kn))\; n_{\chi,{\rm iso}}(r,t) \tag{9}$$

$$\mathfrak{f}(Kn) = 1 - \frac{1}{1+(0.4/Kn)^2} \;.$$

The evolution of the total number of WIMPs in the Sun is governed by the following equation:

$$\dot{N}_\chi(t) = C_\odot - A_\odot\, N_\chi^2(t) - E_\odot\, N_\chi(t)\ , \tag{10}$$

where $C_\odot$ is the capture rate, $A_\odot$ is the annihilation rate and $E_\odot$ is the evaporation rate, which is only relevant for low-mass WIMPs.

For weak cross sections, the capture rate is defined as [37, 38]

$$C_\odot^{\rm weak} = \sum_i \int_0^{R_\odot} 4\pi r^2 dr \int_0^\infty du \left(\frac{\rho_\chi}{m_\chi}\right) \frac{f_{v_\odot}(u)}{u}\, \omega(r) \int_0^{v_e} R_i^-(\omega \to v) |F_i(\omega, v)|^2\, dv\ , \tag{11}$$

where $R_i^-(\omega \to v)$ is the rate at which a WIMP with velocity ω scatters off a Maxwell-Boltzmann distribution of nuclei i, with isotropic and velocity-independent cross section, to a final velocity $v < \omega$ [37]. In order to account for the lack of coherence an exponential form factor $|F_i(\omega, v)|^2$ is included [38]. We consider a WIMP population with a local density $\rho_\chi = 0.3$ GeV/cm^3 and a Maxwell-Boltzmann velocity distribution $f_{v_\odot}(u)$, which as seen by an observer moving at $v_\odot$, the velocity of the Sun with respect to the WIMPs rest frame, is given by

$$f_{v_\odot}(u) = \sqrt{\frac{3}{2\pi}}\, \frac{u}{v_\odot\, v_d} \left[e^{-\frac{3\,(u - v_\odot)^2}{2\, v_d^2}} - e^{-\frac{3\,(u + v_\odot)^2}{2\, v_d^2}} \right]\ , \tag{12}$$

with u being the WIMP velocity at infinity and $\omega^2(r) = u^2 + v_e^2(r)$, where $v_e(r)$ is the escape velocity at a distance r from the center of the Sun. We take the values $\bar{v} = 270$ km/s for the velocity dispersion and $v_\odot = 220$ km/s for the velocity of the Sun with respect to the WIMPs rest frame. In the case of neglecting either the finite temperature or the decoherence effects, analytical solutions for the capture rate per unit volume are known [38]. However, although the effects due to the finite temperature of the nuclei are small, we include them in the calculations (as well as the decoherence).

Nevertheless, Eq. (11) is valid when the scattering cross section is small enough so that the probability of interaction is much smaller than 1. However, the capture rate cannot grow indefinitely with the cross section, for it must saturate to a maximal value set by the geometrical cross section of the Sun (when the probability of interaction is 1). Using Ref. [38], the geometrical capture rate is given by

$$C_\odot^{\rm geom} = \pi R_\odot^2 \left(\frac{\rho_\chi}{m_\chi}\right) \int_0^\infty du\, f_{v_\odot}(u)\, \frac{\omega^2(R_\odot)}{u} = \pi R_\odot^2 \left(\frac{\rho_\chi}{m_\chi}\right) \langle v \rangle_0 \left(1 + \frac{3}{2}\, \frac{v_e^2(R_\odot)}{v_d^2}\right) \xi(v_\odot)\ , \tag{13}$$

where $\langle v\rangle_0 = \sqrt{8/(3\pi)}\, v_d$ is the average velocity in the WIMPs rest frame and the factor $\xi(v_\odot) = 0.81$ takes into account the suppression due to the motion of the Sun. This expression for the geometrical capture rate agrees at a level better than the percent with that obtained in Ref. [39][3]. Thus, we estimate the capture rate as

$$C_\odot = C_\odot^{\rm weak}\, \left(1 - e^{-C_\odot^{\rm geom}/C_\odot^{\rm weak}}\right) \ . \tag{14}$$

The annihilation rate $A_\odot$ is defined as

$$A_\odot = \langle \sigma_A v\rangle\, \frac{\int_0^{R_\odot} 4\pi r^2 dr\, n_\chi^2(r,t)}{\left(\int_0^{R_\odot} 4\pi r^2 dr\, n_\chi(r,t)\right)^2} \ , \tag{15}$$

where $\langle \sigma_A v\rangle$ is the thermal average of the WIMP annihilation cross section times the relative velocity. In this work, we assume an annihilation cross section typical of thermal WIMPs, $\langle \sigma_A v\rangle = 3\cdot 10^{-26}\,{\rm cm}^3/{\rm s}$.

Finally, analogously to the definition of the WIMP distribution, we define the evaporation rate $E_\odot$ as

$$E_\odot = \mathfrak{f}(Kn)\, E_{\odot,{\rm LTE}} + (1 - \mathfrak{f}(Kn))\ E_{\odot,{\rm iso}} \ , \tag{16}$$

where, following Ref. [31],

$$E_{\odot,\lambda} = \sum_i \int_0^{R_\odot} 4\pi r^2\, s(r)\, dr \int_0^\infty d\omega\, f_\odot(\omega, T(r)) \int_{v_e}^\infty R_i^+(\omega \to v) dv \ , \tag{17}$$

where the rate at which a WIMP with velocity ω scatters off a Maxwell-Boltzmann distribution of nuclei i, with isotropic and velocity-independent cross section, to a final velocity $v > \omega$ is given by $R_i^+(\omega \to v)$ [37]. We assume that WIMPs have a truncated thermal distribution $f_\odot(\omega, T(r))$ with a cutoff[4] at $\omega = v_e$ where $T(r) = T_\chi$ ($T(r) = T_\odot(r)$) for $\lambda = $ iso ($\lambda = $ LTE). The suppression factor $s(r)$ accounts for the fraction of WIMPs that, after reaching the escape velocity, would actually escape from the Sun. We have slightly modified the estimate of Ref. [31] to allow for a smooth transition between the optically thin and thick regimes and have defined it as

$$s(r) = \frac{7}{10}\, \frac{1 - e^{-10\,\tau(r)/7}}{\tau(r)}\, e^{-\tau(r)} \ , \tag{18}$$

[3] Note that there is a typo in Eq. (26) of Ref. [39]: the factor (M_i/m_i) should not be there.

[4] Note that if the cutoff velocity is smaller than v_e, the evaporation rate would be suppressed with respect to the case usually considered and that we follow here [37]. This is a conservative approach, for a lower evaporation rate would allow to set better limits for low WIMP masses.

where $\tau(r) = \int_r^{R_\odot} \ell(r')^{-1}\, dr'$ is the optical depth.

In our computations we use the analytical solution for the evaporation rate per unit volume obtained in Ref. [37] and add the suppression factor as indicated above. This suppression is only relevant in the optically thick regime, but indeed it results on the evaporation mass (the minimum mass for WIMPs to be trapped in the Sun) to *decrease* with the scattering cross section, which is the opposite behavior to the one in the optically thin regime. In other words, the evaporation mass has a maximum at a value of the scattering cross section around the transition between the two regimes. This was first noted by Ref. [31] and has an important impact on our results.

Once all the ingredients are computed, the WIMPs annihilation rate is given by $\Gamma = A_\odot\, N_\chi^2/2$ and the solution of Eq. (10) today ($t = t_\odot = 4.57$ Gyr) reads [9, 40]

$$\Gamma(m_\chi, \sigma_\chi) = \frac{1}{2}\, C_\odot \left(\frac{\tanh(\kappa\, t_\odot/\tau_E)}{\kappa + \frac{1}{2}\, E_\odot\, \tau_E\, \tanh(\kappa\, t/\tau_E)} \right)^2 , \tag{19}$$

where $\tau_E = (A_\odot C_\odot)^{-1/2}$ is the equilibration time scale in the absence of evaporation and $\kappa = (1 + (E_\odot \tau_E/2)^2)^{1/2}$. For a thermal annihilation cross section and for the scattering cross sections under consideration, equilibrium is always reached ($t_\odot >> \tau_E$, $\tanh(\kappa\, t_\odot/\tau_E) \simeq 1$), although in our computations we keep the exact Eq. (19).

III. MEV NEUTRINOS FROM WIMPS ANNIHILATIONS IN THE SUN

Being produced in a very dense medium, among all the final products of WIMPs annihilations, only neutrinos can escape. So far, all previous works have focused on the high-energy neutrino flux resulting from the subsequent hadronization, fragmentation and decay of the final states in heavy quarks, gauge bosons or $\tau^+\tau^-$ channels, and have disregarded annihilations into e^+e^-, $\mu^+\mu^-$ or light quarks because they would only produce (if any) a flux of low-energy neutrinos from pion and muon decay at rest. These MeV neutrinos are the focus of this work.

The propagation of the annihilation products of WIMPs annihilations in the Sun would produce pions that would be stopped and could subsequently decay at rest, giving rise to a monochromatic neutrino spectrum at 29.8 MeV. Practically all π^-, after stopping, would be captured in an atomic orbit and promptly the nucleus would de-excite by emitting X-rays or transferring energy to Auger electrons. After that, the π^- would get absorbed by the

nucleus without decaying in processes of the type of $\pi^- NN \to NN$, where N represents a nucleon. Hence, only neutrinos from π^+ decays would contribute significantly to the low-energy neutrino flux. Let us note that the propagation of high-energy e^-/e^+ would also produce small amounts of pions, so this could open up the possibility to use this low-energy neutrino flux to constrain WIMPs annihilations into e^+e^-. In addition, all muons produced in pion decays, in the leptonic decay modes of hadrons or taus and in the case of direct annihilations into $\mu^+\mu^-$, are stopped in the dense region where they are produced and decay at rest. Thus, in addition to the monochromatic spectrum from π^+ decays at rest, neutrinos from μ^+ and μ^- decaying at rest would also contribute (with a well known spectrum below 52.8 MeV) to the final low-energy neutrino flux. Hence, the sources of the flux of neutrinos studied here are

$$\begin{aligned}
\pi^+ &\to \mu^+ + \nu_\mu \ , \\
\pi^- &\to \mu^- + \bar{\nu}_\mu \quad (\textit{negligible contribution}) \ , \\
\mu^+ &\to e^+ + \nu_e + \bar{\nu}_\mu \ , \\
\mu^- &\to e^- + \bar{\nu}_e + \nu_\mu \ .
\end{aligned} \tag{20}$$

The shape of the spectra of these neutrinos is well known and, in order to calculate the relative contributions of each type of neutrino spectrum to the final neutrino spectrum, we simulate all the particles propagation with GEANT4 [41, 42]. To determine for each WIMP mass the average density and composition of the medium where the products of WIMPs annihilations propagate, we use the SSM [27, 28] and the WIMP distribution in the Sun (as a function of the WIMP mass), given in Eq. (9), to compute it. Thus, for each WIMP mass, we obtain the average density and solar composition of the region where WIMPs accumulate and annihilate. In Fig. 1 we show the radial distribution of the number density of WIMPs in the Sun normalized to its value at the solar center, $n_\chi(r,t)/n_\chi(0,t)$, (left panel) and the weighted density and composition of the Sun in the WIMPs environment (right panel).

For the simulations, we proceed as follows. For the case of WIMPs annihilating into a pair of leptons we inject the two leptons with energies equal to the WIMP mass directly into GEANT4 and let them propagate and decay. In the case of WIMPs annihilations into quarks, we use PYTHIA 6.4 [43] to hadronize and fragment the initial quarks and do not let decay any of the final particles that are produced. Then, we inject into GEANT4 the full spectrum of all the produced particles and simulate their propagation in the Sun. Finally,

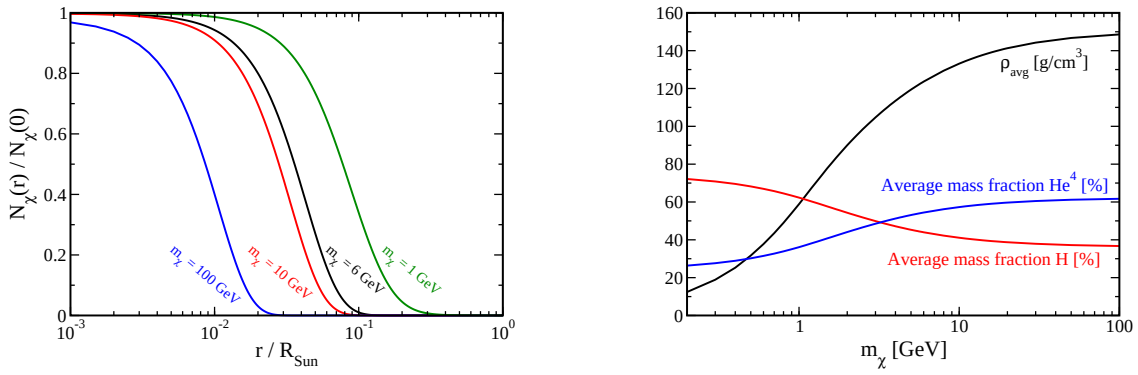

Figure 1: ***Left panel: Distribution of the number density of WIMPs in the Sun*** *(normalized to the density at the center of the Sun), $n_\chi(r,t)/n_\chi(0,t)$, as a function of the distance to the center of the Sun for four WIMP masses.* ***Right panel: Weighted density and composition of the Sun****, according to the SSM [27, 28] and to the distribution of WIMPs (left panel), as a function of the WIMP mass. We only show the two main elements, He^4 and H. Here, we have assumed a spin-dependent cross section, $\sigma_p^{SD} = 10^{-40}$ cm^2, although the results are almost the same for any other case.*

we count the number of π^+, π^-, μ^+ and μ^- that decay at rest (we also count all π^-, which are not captured and decay at rest, although their number is negligible). These numbers represent the relative weights for each of the types of neutrino and antineutrino spectra (four from muon decay and two from pion decay) indicated in Eq. (20), which allow us to compute the initial electron and muon neutrino and antineutrino fluxes at the source.

The final number of neutrinos and antineutrinos from pion and muon decay at rest can be understood from Fig. 2 where we show different results for WIMPs annihilations into light quarks and tau leptons. In the left panel, we show the number of π^+ (solid lines) and their average energy (dashed lines) just after WIMPs annihilations (before propagation) as a function of the WIMP mass; in the middle panel, the number of π^+ (solid lines) and π^- (dashed lines) produced after the propagation of one π^+ (black lines) or one π^- (red lines) as a function of the energy of the initial pion; and in the right panel, the number of neutrinos and antineutrinos from π^+ and μ^+ decay at rest as a function of the WIMP mass. From the left panel we see that, whereas the number of π^+ produced (before propagation of the products of annihilation) in the case of annihilations into light quarks grows with the WIMP mass and in the case of annihilations into tau leptons it remains approximately constant,

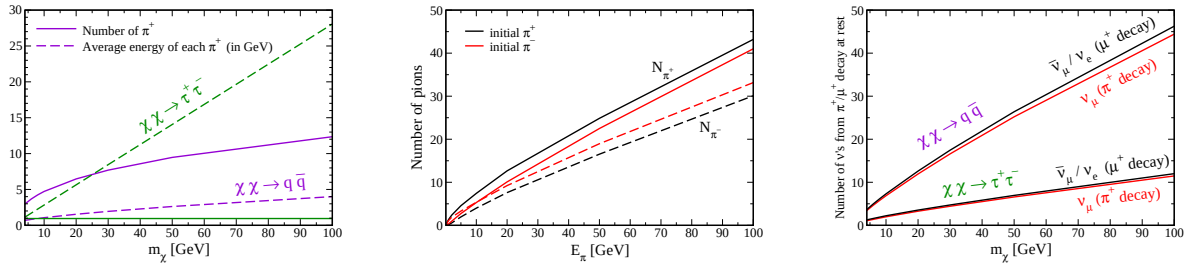

Figure 2: ***Left panel: Number of*** π^+ ***(solid lines) and their average energy (dashed lines)*** *just after WIMPs annihilations (before propagation) as a function of the WIMP mass.* ***Middle panel: Number of*** π^+ ***(solid lines) and*** π^- ***(dashed lines) produced after the propagation of one*** π^+ ***(black lines) or one*** π^- ***(red lines)*** *as a function of the energy of the initial pion.* ***Right panel: Number of neutrinos and antineutrinos from*** π^+ ***and*** μ^+ ***decay at rest*** *as a function of the WIMP mass. In the three panels, we show the results for two annihilation channels,* $\chi\chi \to q\bar{q}$ *and* $\chi\chi \to \tau^+\tau^-$*. We have considered an average density and composition of the region where WIMPs annihilation occur corresponding to* $m_\chi = 100$ *GeV.*

the average energy of these pions increases faster with the WIMP mass in the latter case. Overall, convolving this result with that in the middle panel, this behavior implies a faster increase on the final number of neutrinos for WIMPs annihilations into light quarks than into tau leptons (see right panel), and hence better limits in the former case, as discussed below.

These neutrinos would then propagate from the Sun to the Earth and would be detected via the charged-current interactions of those arriving at the detector in the electron flavor (see below). In order to calculate the electron neutrino and antineutrino fluxes at the Earth, one should take into account that neutrinos mix. For the energies of interest (above 10 MeV) neutrinos propagate adiabatically in the Sun and at the region where they are produced matter effects are dominant, so ν_e ($\bar{\nu}_e$) exit the Sun as almost purely ν_2 (ν_1) and ν_μ ($\bar{\nu}_\mu$) almost as an equal mixture of ν_1 (ν_2) and ν_3. Hence, the probabilities for neutrinos

to arrive at the Earth in the electron flavor are

$$
\begin{aligned}
P(\nu_\mu \to \nu_e) &= \sin^2\theta_{13}\,\cos^2\theta_{13}\,\sin^2\theta_{12}\,(1+\sin^2\theta_{12}) + \cos^2\theta_{23}\,\cos^2\theta_{12}\,\cos^2\theta_{13} \simeq 0.35\ , \\
P(\bar\nu_\mu \to \bar\nu_e) &= \sin^2\theta_{13}\,\cos^2\theta_{13}\,\sin^2\theta_{12}\,(1+\cos^2\theta_{12}) + \cos^2\theta_{23}\,\sin^2\theta_{12}\,\cos^2\theta_{13} \simeq 0.17\ , \\
P(\nu_e \to \nu_e) &= \sin^2\theta_{12}\,\cos^2\theta_{13} + \sin^4\theta_{13} \simeq 0.31\ , \\
P(\bar\nu_e \to \bar\nu_e) &= \cos^2\theta_{12}\,\cos^2\theta_{13} + \sin^4\theta_{13} \simeq 0.66\ . \qquad (21)
\end{aligned}
$$

The final electron neutrino and antineutrino spectra at the detector are obtained by combining the initial fluxes with the above probabilities[5]. We use the values of the mixing angles (for normal hierarchy) from Ref. [46].

IV. DETECTION OF MEV NEUTRINOS WITH SK

SK is a water Čerenkov detector with a fiducial volume of 22.5 ktons ($1.5{\cdot}10^{33}$ free protons and $7.5\cdot10^{32}$ oxygen nuclei). For energies below 52.8 MeV, the best present data come from the search for the DSNB [21, 22], which is split into three phases: SK-I ($t_I = 1497$ days), SK-II ($t_{II} = 794$ days) and SK-III ($t_{III} = 562$ days). The recent analysis [21, 22] has substantially improved over the previous one [47, 48], with better efficiencies, lower energy thresholds and almost twice as much statistics.

The signal at SK is the detection of the positrons (electrons) produced in $\bar\nu_e$ (ν_e) charged-current interactions in the detector below ~ 100 MeV. At these energies, the inverse beta-decay cross section ($\bar\nu_e\, p \to n\, e^+$) is about two orders of magnitude larger than the $\nu{-}e$ elastic scattering cross section. Below ~ 80 MeV, this is the dominant interaction of $\bar\nu_e$. Although the WIMP signal discussed in this work is below this energy, we have also taken into account the interactions of ν_e and $\bar\nu_e$ off oxygen nuclei, which give non-negligible contributions to the lowest energy bins.

The low energy threshold in the analysis is determined by the ability to remove the radioactive spallation caused by cosmic-ray muons hitting an oxygen nucleus. An improved spallation cut has allowed to reduce the energy threshold used in the previous analysis down to 16 MeV (17.5 MeV) for SK-I/III (SK-II). In addition to this, a number of other cuts were

[5] We neglect the correction due to the Earth-matter effect [44, 45], which after averaging over all possible trajectories we expect it to be at the percent level. Moreover, the SK collaboration did not take this into account when simulating the backgrounds and we use their results in our analysis.

performed, as noise reduction, fiducial volume, solar angle, incoming event, decay electron, pion, Čerenkov angle and other cuts [21, 22]. The maximum energy in the recent SK analysis is 88 MeV, which is also higher than in the previous one.

In this energy range, the two dominant backgrounds which remain after the cuts are the atmospheric ν_e and $\bar{\nu}_e$ background and, mainly, the Michel positrons (electrons) from the decays of low energy muons, produced by atmospheric $\bar{\nu}_\mu$ (ν_μ) with typical energies of about ∼200 MeV, which are below detection threshold, the so-called invisible muons[6]. These muons are slowed down rapidly and subsequently decay, mimicking the signal from ν_e or $\bar{\nu}_e$, but with a spectrum whose shape is very well known.

In addition to these two backgrounds, in the new SK analysis two extra sources of background were considered: neutral current (NC) elastic events, which give rise to de-excitation gammas or produce other reactions, and low energy muons and pions misidentified as electrons/positrons.

In the new SK analysis three Čerenkov angle regions are defined: $20° - 30°$ (the 'low angle' or 'μ/π' region), $38° - 50°$ (the 'signal' region) and $78° - 90°$ (the 'high angle' or 'NC elastic' region). Inverse beta-decay positrons in the data sample (with energies above 16 MeV) are highly relativistic and have a Čerenkov angle of around 42°. On the other hand, low energy muons and pions travel more slowly and emit light with a smaller Čerenkov angle. In addition, some other events with more isotropic nature can have higher Čerenkov angles, such as events with multiple gammas.

V. ANALYSIS

In this work, we follow some parts of the analysis performed in Refs. [49, 50], although we update some aspects following the new SK analysis [21, 22], as we explain below.

We have considered both the interactions of $\bar{\nu}_e$ off free protons and the interactions of ν_e and $\bar{\nu}_e$ off bound nucleons. At very low energies, the inverse beta-decay reaction relates the energy of the outgoing positron to that of the incoming $\bar{\nu}_e$, such that $E_{e^+} \simeq E_{\bar{\nu}} - 1.3$ MeV. However, at higher energies, corrections of the order of $\mathcal{O}(E_{\bar{\nu}}/\mathrm{M_N})$, where $\mathrm{M_N}$ is the nucleon mass, become important and the spread in positron energy is, to first order, given by $\Delta E_{e^+} \approx$

[6] If the momentum of the produced muon is below ∼120 MeV, then the muon is below the threshold for emitting Čerenkov radiation in water.

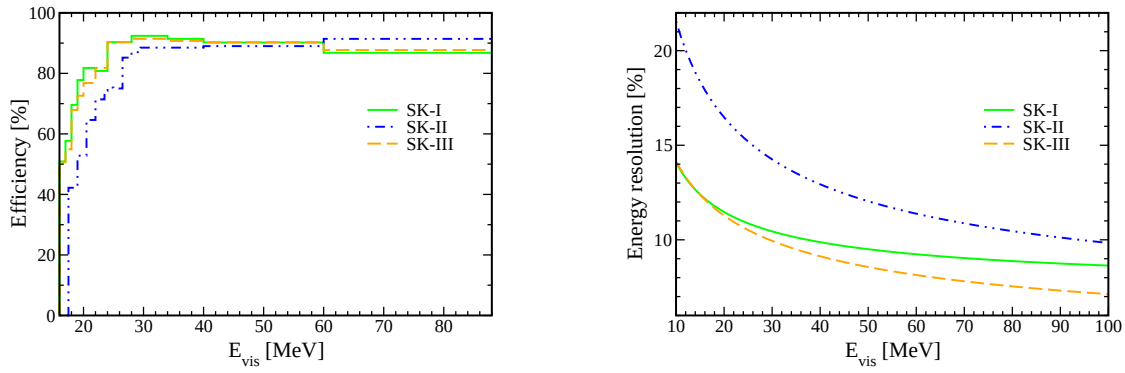

Figure 3: ***Efficiency [21, 22] (left panel) and energy resolution [54–56] (right panel) of each SK phase*** *as a function of the visible (detected positron or electron) energy,* $E_{\rm vis}$.

$2E_{\bar{\nu}}^2/\mathrm{M_N}$. For the inverse beta-decay reaction we use the full cross section [51, 52] and for the interactions off bound nucleons, we consider a relativistic Fermi gas model [53] with a Fermi surface momentum of 225 MeV and a binding energy of 27 MeV. For each of the three SK phases, we have used the corresponding energy-dependent efficiencies [21, 22] and a Gaussian energy resolution function [54–56] of width $\sigma(E_e)$, $R(E_e, E_{\rm vis})$ (shown in Fig. 3), with E_e and $E_{\rm vis}$ being the incoming and detected electron/positron energy, respectively.

The expected fraction of the low-energy neutrino signal from WIMPs annihilations in the Sun in the visible electron/positron energy interval $E_{\rm vis} = [E_l, E_{l+1}]$ is given by

$$A_l = A_s \int dE_e\, dE_\nu\, G_l(E_e) \;\times\; \left[\left(\frac{d\sigma_{\rm f}^{\bar{\nu}_e}}{dE_e}(E_{\bar{\nu}_e}, E_e) + \frac{1}{2}\,\frac{d\sigma_{\rm b}^{\bar{\nu}_e}}{dE_e}(E_{\bar{\nu}_e}, E_e)\right)\frac{d\Phi^{\bar{\nu}_e}}{dE_{\nu_e}}(E_{\bar{\nu}_e}) + \frac{1}{2}\,\frac{d\sigma_{\rm b}^{\nu_e}}{dE_e}(E_\nu, E_e)\,\frac{d\Phi^{\nu_e}}{dE_{\nu_e}}(E_{\nu_e})\right] , \tag{22}$$

with $E_1 = 16$ MeV and $E_{l+1} - E_l = 4$ MeV. A_s is a normalization constant so that $\sum A_l = 1$. The neutrino cross sections off free nucleons and off nuclei (bound nucleons) are given by $\sigma_{\rm f}$ and $\sigma_{\rm b}$, respectively, and the factor 1/2 is due to water having twice as many free protons as oxygen nuclei. The effects of the energy resolution function are embedded in $G_l(E_e) = \int_{E_l}^{E_{l+1}} \epsilon(E_{\rm vis})\, R(E_e, E_{\rm vis})\, dE_{\rm vis}$, with $\epsilon(E_{\rm vis})$ the efficiency in that energy bin. The

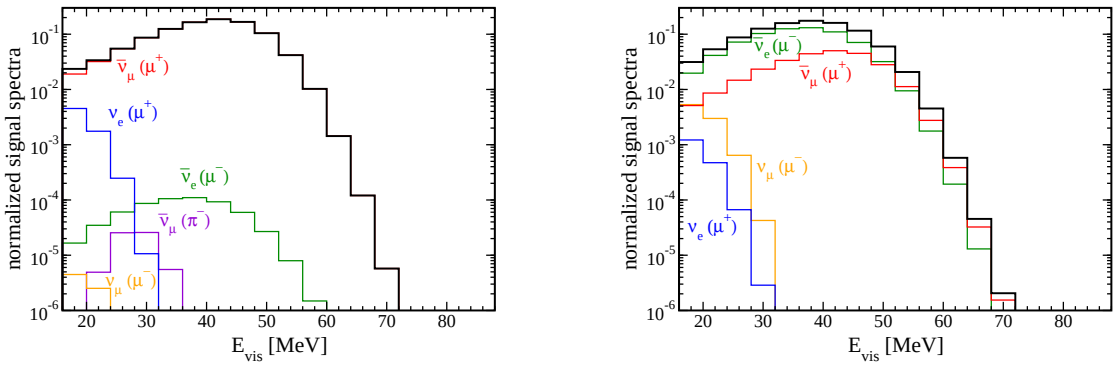

Figure 4: ***Normalized signal spectra*** *in the region of observation for WIMPs annihilations into light quarks (left panel) and $\mu^+\mu^-$ (right panel), for $m_\chi = 6$ GeV and SK-I. The colored lines represent the different contributions to the final neutrino spectra from pion (in the left panel) and muon decay (in both panels) at rest and the thick black line represents the total spectrum.*

fluxes of electron neutrinos and antineutrinos at the detector are given by

$$\frac{d\Phi^{\nu_e}}{dE_{\nu_e}}(E_{\nu_e}) = \frac{1}{4\pi d_\odot^2}\,\Gamma(m_\chi,\sigma_\chi)\left(P(\nu_e\to\nu_e)\,\frac{dF}{dE_{\nu_e}}(E_{\nu_e}) + P(\nu_\mu\to\nu_e)\,\frac{dF}{dE_{\nu_\mu}}(E_{\nu_\mu})\right)$$
$$\frac{d\Phi^{\bar\nu_e}}{dE_{\bar\nu_e}}(E_{\bar\nu_e}) = \frac{1}{4\pi d_\odot^2}\,\Gamma(m_\chi,\sigma_\chi)\left(P(\bar\nu_e\to\bar\nu_e)\,\frac{dF}{dE_{\bar\nu_e}}(E_{\bar\nu_e}) + P(\bar\nu_\mu\to\bar\nu_e)\,\frac{dF}{dE_{\bar\nu_\mu}}(E_{\bar\nu_\mu})\right) \quad ,(23)$$

where $d_\odot$ is the average distance Sun-Earth and dF/dE_{ν_e} and $dF/dE_{\bar\nu_e}$ (dF/dE_{ν_μ} and $dF/dE_{\bar\nu_\mu}$) are the electron (muon) neutrino and antineutrino spectra per WIMPs annihilation in the Sun. We show in Fig. 4 the normalized signal spectra of the different contributions to the final neutrino spectra in the interval $E_{\rm vis} = [16-88]$ MeV for the case of WIMPs annihilations into light quarks (left panel) and $\mu^+\mu^-$ (right panel), for $m_\chi = 6$ GeV and SK-I.

In order to obtain the upper limit on the WIMP-nucleon scattering cross section, we use the recent data reported by the SK collaboration [21, 22]. We consider the four types of background described above and fit the data in the three Čerenkov angle regions defined in the SK analysis [21, 22]. In order to do so, we use the probability distribution functions (PDF) provided in Ref. [22], which include the relative normalizations among the three Čerenkov regions for each background and each SK phase. In the analysis we leave the normalizations of the four backgrounds and the signal free in each Čerenkov region, but

with the relative normalizations among regions kept fixed. We fit the total number of events of each type, α (WIMP signal), β (invisible muons background), γ (atmospheric ν_e background), δ (NC elastic background) and η (μ/π background). We consider 18 4-MeV bins (in the interval 16-88 MeV) and perform an extended maximum likelihood fit. We obtain the best fit as the combination of parameters that maximizes the likelihood, defined as

$$\mathcal{L} = e^{-(\alpha+\beta+\gamma+\delta+\eta)} \prod_{a=1}^{3} \prod_{l=1}^{18} \frac{[(\alpha \cdot A_l^a) + (\beta \cdot B_l^a) + (\gamma \cdot C_l^a) + (\delta \cdot D_l^a) + (\eta \cdot E_l^a)]^{N_l^a}}{N_l^a!} \ , \quad (24)$$

where the product a is over the three Čerenkov regions, the product l is over all energy bins, N_l^a is the number of detected events in the l-th bin in region a, and A_l^a, B_l^a, C_l^a, D_l^a and E_l^a are the fractions (so that for each case the total is normalized to 1 over the three regions) of the WIMPs annihilation signal, Michel positrons and electrons from muon decay, atmospheric ν_e- and $\bar{\nu}_e$-induced spectra, NC elastic events and misidentified muons and pions, that are in the l-th bin and in the a Čerenkov region, respectively. The fractions $A_l^{\rm signal}$ in the signal region are calculated using the $\bar{\nu}_e$ and ν_e low-energy fluxes from WIMP annihilations in the Sun as described above[7]. We have reproduced the PDFs in the signal region for the two main backgrounds and our results are in perfect agreement with the SK results. In order to reproduce $B_l^{\rm signal}$ and $C_l^{\rm signal}$ we have used the atmospheric neutrino flux calculation with FLUKA [57, 58], and for $B_l^{\rm signal}$ we have taken into account that 18.4% of the μ^- are stopped in water, so the spectrum of their decay electron gets distorted.

We have also included the energy-independent efficiency systematic error by modifying the likelihood in the way described in Refs. [21, 22], with a total error different for each of the data-taking phases. The final likelihood is maximized for each SK phase separately, so that it remains as a function of just α, the number of signal events (the best fit event spectra and data for $m_\chi = 6$ GeV and SK-I are shown in the left panels of Fig. 5 for the case of WIMPs annihilations into light quarks and $\mu^+\mu^-$). Finally, the three likelihoods are calculated as a function of the number of signal events/year, $\tilde{\alpha}$, and multiplied (shown in the right panels of Fig. 5 for the case of WIMPs annihilations into light quarks and $\mu^+\mu^-$,

[7] As the spectrum of the WIMP signal is similar to that of the invisible muons background, we have estimated the signal in the three Čerenkov angle regions as $A_l^a \propto A_l^{\rm signal} \times B_l^a/B_l^{\rm signal}$ and then properly normalized to 1 over the three regions. Nevertheless, we get the same results if we assume that the events from WIMPs annihilations are only in the signal region.

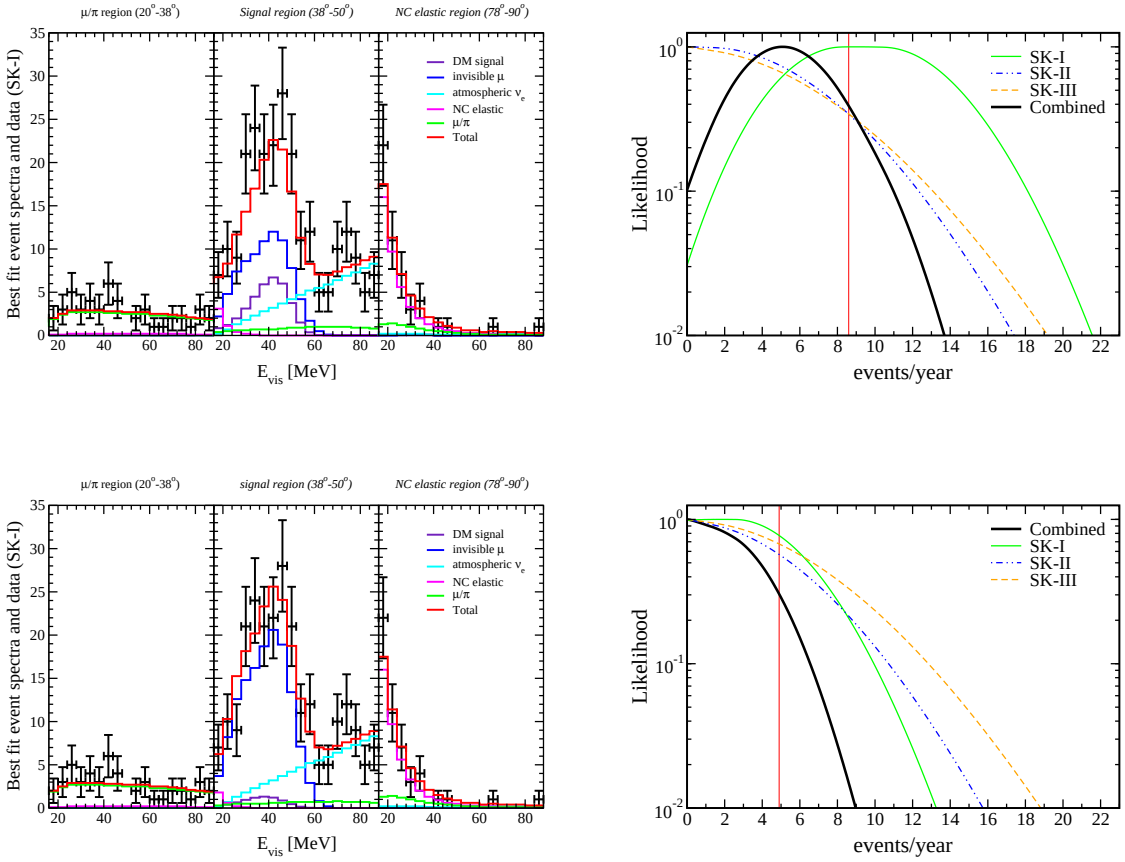

Figure 5: ***Left panels: Best fit event spectra and data [21, 22]*** *for SK-I in the three Čerenkov angle regions. The two main backgrounds in the signal region, invisible muons and atmospheric ν_e and $\bar{\nu}_e$, are the blue and cyan histograms, respectively. The μ/π and NC elastic backgrounds are depicted by the green and magenta histograms, respectively. The WIMP signal spectra is the violet histogram and the total best fit spectra is the red histogram.* ***Right panels: Likelihood normalized to its maximum*** *for each SK phase and for the combined analysis, as a function of the number of events per year. The vertical line represents the 90% CL limit for the combined fit.* ***Upper (lower) panels*** *are for the case of WIMPs annihilations into light quarks ($\mu^+\mu^-$) and $m_\chi = 6$ GeV. Note that in the upper panel the combined best fit is 5.1 signal events.*

for $m_\chi = 6$ GeV). The 90% confidence level (CL) limit on the number of signal events/year, $\tilde{\alpha}_{90}$, is determined by

$$\frac{\int_0^{\tilde{\alpha}_{90}} \mathcal{L}_{\rm tot}(\tilde{\alpha})\, d\tilde{\alpha}}{\int_0^{\infty} \mathcal{L}_{\rm tot}(\tilde{\alpha})\, d\tilde{\alpha}} = 0.9 \ . \tag{25}$$

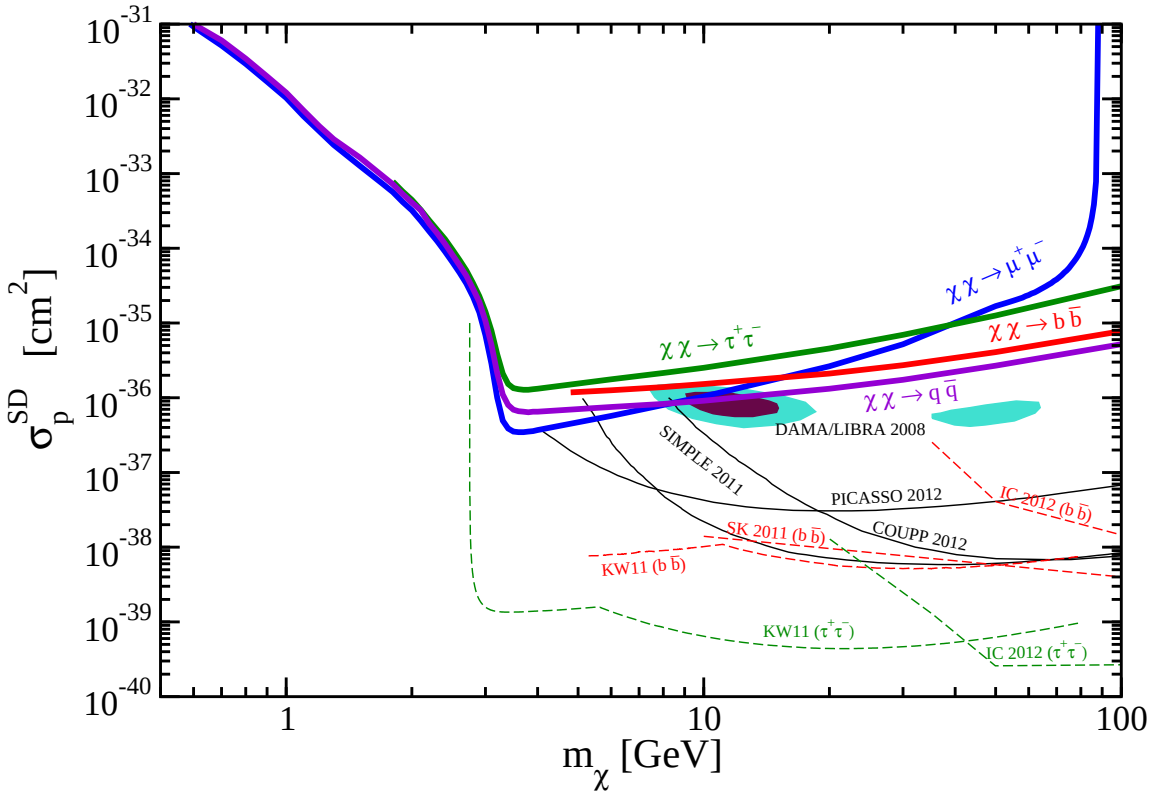

Figure 6: ***Limits on the spin-dependent scattering cross section of WIMPs off protons at 90% CL for different annihilation channels.*** *The limits from SIMPLE [59], PICASSO [60] and COUPP [61] are shown with black lines. The limits from SK searches of GeV neutrinos (for different data sets) are depicted for two annihilation channels [62, 63], as well as those from IceCube [64]. The DAMA/LIBRA [65, 66] regions (at 90% CL and 3σ CL) are also shown as interpreted in Refs. [67, 68].*

The 90% CL limit on the scattering cross section, σ_χ^{90}, is then obtained by solving

$$\Gamma(m_\chi, \sigma_\chi^{90})\, A^{\rm tot} = \tilde{\alpha}_{90} \quad , A^{\rm tot} \equiv \frac{\sum_{SK} A^{SK} t_{SK}}{\sum_{SK} t_{SK}}\,, \tag{26}$$

where A^{SK} is the number of events per WIMPs annihilation for each SK phase at the detector.

The results for spin-dependent (off protons) and spin-independent cross sections are shown in Figs. 6 and 7, respectively, along with the bounds from direct detection searches

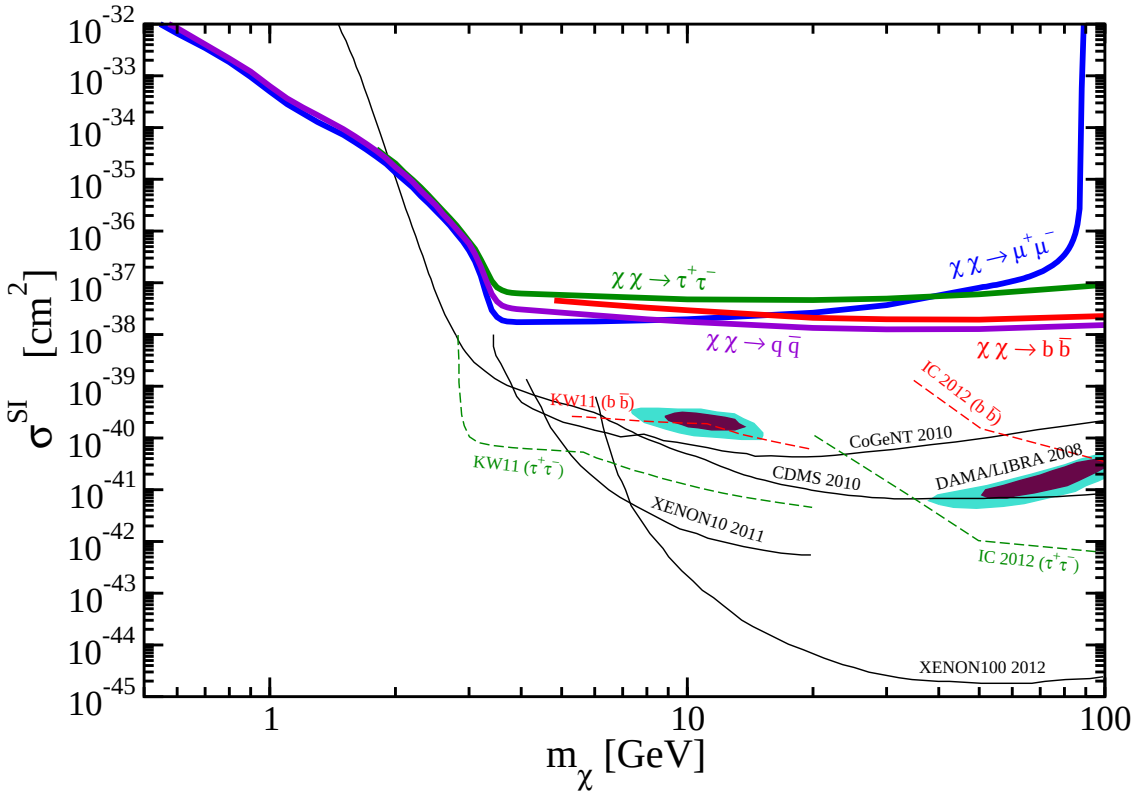

Figure 7: ***Limits on the spin-independent scattering cross section of WIMPs at 90% CL for different annihilation channels.*** *The limits from CoGeNT [69], CDMS [70], XENON10 [71] and XENON100 [72] are shown with black lines. The limits from SK searches of GeV neutrinos are depicted for two annihilation channels [62, 63], as well as those from IceCube [64]. The DAMA/LIBRA [65, 66] regions (at 90% CL and 3σ CL) are also shown as interpreted in Refs. [67, 68].*

and the analysis of GeV neutrinos from WIMPs annihilations in the Sun detected at SK. The most stringent bounds we obtain on the spin-dependent (spin-independent) cross section are for WIMPs annihilations into light quarks for $m_\chi > 8.4$ GeV ($m_\chi > 8.6$ GeV) and for annihilations into $\mu^+\mu^-$ for lower masses. Whereas for spin-independent, the limits are a few orders of magnitude weaker than the ones obtained with direct searches for m_χ above a few GeV, for spin-dependent, they are comparable to (or even more stringent than) them just below $m_\chi \simeq 10$ GeV. We note that, in this case, the limits for WIMPs annihilations into

quarks or $\mu^+\mu^-$ exclude part of the DAMA/LIBRA region [65, 66] at 90% CL. In addition, it is important to note that below $m_\chi = 4.1$ GeV ($m_\chi = 2.0$ GeV) the limits we obtain for the spin-dependent (spin-independent) cross section are more constraining than any direct detection result and extend to the kinematical limits of each annihilation channel (not shown on the plots for all the cases), albeit only reaching relatively large values. In the optically thick regime ($\sigma_{\rm p}^{\rm SD} \gtrsim 10^{-35}$ cm^2 and $\sigma^{\rm SI} \gtrsim 3 \times 10^{-37}$ cm^2) evaporation is much less effective, because upscattered WIMPs above the escape velocity have a very short mean free path and are kept trapped inside the Sun. Although first noted in Ref. [31], this is usually overlooked in the literature and it is usually assumed that WIMPs below a few GeV cannot get trapped in the Sun.

Although e^+e^- interactions with the solar medium would generate a modest amount of pions, which subsequently produce MeV neutrinos, current data are compatible at 90% CL with the maximum possible signal from this channel, obtained for the saturation value of the capture rate. Finally, let us note that the limit for the $\mu^+\mu^-$ channel above the evaporation mass follows the dependence of the capture rate with the WIMP mass, for the initial muons are always stopped and thus, regardless the WIMP mass, the final number of muons decaying at rest per WIMPs annihilation is two. For $m_\chi > 90$ GeV, the capture rate is equal to its geometrical value, so the sensitivity decreases drastically (for low masses the effect is more involved because evaporation is also important). On the other hand, for the $\tau^+\tau^-$ channel, below some mass, the number of muons decaying at rest is smaller because a fraction of taus goes to electrons and all the produced π^- get absorbed without decaying. However, the passage through the solar medium of the products of tau decay gives rise to a number of neutrinos that increases (almost linearly) with energy and hence, with the WIMP mass (a similar behavior is observed for the case of WIMPs annihilations into quarks). This explains why these limits cross each other. Another factor being the slightly more constraining fit for the $\mu^+\mu^-$ case (see Fig. 5).

VI. CONCLUSIONS

The potential signal of GeV neutrinos produced after WIMPs annihilations in the Sun has been extensively studied so far [10–20], although these searches do not consider annihilations into light quarks, $\mu^+\mu^-$ or e^+e^-, for these channels do not produce GeV neutrinos. However,

the propagation in the Sun of the products of WIMPs annihilations into quarks or leptons would always produce pions and muons that after being stopped would decay at rest. In this work, we have considered these MeV neutrinos from pion and muon decay at rest, which represents a novel way of constraining WIMPs annihilations in the Sun and, indeed, the only way to set bounds on WIMP annihilations in the Sun if they are into light quarks (except for the case of very high WIMP masses), $\mu^+\mu^-$ or e^+e^-. In order to do so, we have used the SK data on the DSNB [21, 22] and have performed an analogous analysis. It is important to note that taking into account the suppression of the WIMP evaporation rate from the Sun for large scattering cross sections, allows us to set bounds for very low WIMP masses, unlike what is usually assumed within this context.

Our results, Figs. 6 and 7, show that, mainly for low WIMP masses and spin-dependent cross sections, these new limits are competitive with those from direct searches in the few GeV region and extend to the kinematical limits of each annihilation channel. However, SK data do not allow us to set limits on annihilations into e^+e^- yet. In addition, note that direct detection limits are very sensitive to the unknown high-velocity tail of the WIMPs distribution with uncertainties of up to two orders of magnitude in the predicted rates [73, 74]. Hence, in this respect our limits, being little affected by these systematics, are more robust.

It is interesting to also point out that, although the angular distribution of inverse beta-decay events is quite flat, this could in principle be exploited to further constrain this signal [23]. In addition, the angular information of each event could be used to exploit the Earth matter effect [44, 45] as well, on an event by event basis. Finally, let us stress that future detectors such as Hyper-Kamiokande [75] could allow us to improve these limits by up to two orders of magnitude.

Acknowledgments

We thank K. Bays and C. Peña-Garay for providing us with useful information about the SK DSNB analysis and about the SSM, respectively. We would also like to thank M. Vicente-Vacas for discussions, J. Casanellas for rising an important point and M. Sorel for encouragement. SPR thanks the Galileo Galilei Institute for Theoretical Physics, where parts of this work were carried out, for hospitality. NB is supported by the DFG TRR33

'The Dark Universe'. JMA is supported by the Spanish Grant CONSOLIDER-Ingenio 2010 CSD2008-0037 (CUP) of the MINECO. SPR is supported by the Spanish Grant FPA2011-23596 of the MINECO and by the Portuguese FCT through CERN/FP/123580/2011 and CFTP-FCT UNIT 777, partially funded through POCTI (FEDER).

---

[1] G. Jungman, M. Kamionkowski, and K. Griest, "Supersymmetric dark matter", *Phys. Rept.* **267** (1996) 195, arXiv:hep-ph/9506380.

[2] L. Bergström, "Non-baryonic dark matter: Observational evidence and detection methods", *Rept. Prog. Phys.* **63** (2000) 793, arXiv:hep-ph/0002126.

[3] C. Muñoz, "Dark matter detection in the light of recent experimental results", *Int. J. Mod. Phys.* **A19** (2004) 3093, arXiv:hep-ph/0309346.

[4] G. Bertone, D. Hooper, and J. Silk, "Particle dark matter: Evidence, candidates and constraints", *Phys.Rept.* **405** (2005) 279–390, arXiv:hep-ph/0404175 [hep-ph].

[5] G. Bertone, ed., *Particle dark matter: Observations, models and searches.* Cambridge University Press, 2010.

[6] J. Silk, K. A. Olive, and M. Srednicki, "The photino, the Sun and high-energy neutrinos", *Phys.Rev.Lett.* **55** (1985) 257–259.

[7] M. Srednicki, K. A. Olive, and J. Silk, "High-energy neutrinos from the Sun and cold dark matter", *Nucl.Phys.* **B279** (1987) 804.

[8] J. S. Hagelin, K. Ng, and K. A. Olive, "A high-energy neutrino signature from supersymmetric relics", *Phys.Lett.* **B180** (1986) 375.

[9] T. Gaisser, G. Steigman, and S. Tilav, "Limits on cold dark matter candidates from deep underground detectors", *Phys.Rev.* **D34** (1986) 2206.

[10] M. Kamionkowski, "Energetic neutrinos from heavy neutralino annihilation in the Sun", *Phys.Rev.* **D44** (1991) 3021–3042.

[11] A. Bottino, V. de Alfaro, N. Fornengo, G. Mignola, and M. Pignone, "Indirect search for neutralinos at neutrino telescopes", *Phys.Lett.* **B265** (1991) 57–63.

[12] F. Halzen, T. Stelzer, and M. Kamionkowski, "Signatures of dark matter in underground detectors", *Phys.Rev.* **D45** (1992) 4439–4442.

[13] L. Bergström, J. Edsjö, and P. Gondolo, "Indirect neutralino detection rates in neutrino

telescopes", *Phys.Rev.* **D55** (1997) 1765–1770, arXiv:hep-ph/9607237 [hep-ph].

[14] V. D. Barger, F. Halzen, D. Hooper, and C. Kao, "Indirect search for neutralino dark matter with high-energy neutrinos", *Phys.Rev.* **D65** (2002) 075022, arXiv:hep-ph/0105182 [hep-ph].

[15] M. Cirelli, N. Fornengo, T. Montaruli, I. A. Sokalski, A. Strumia, and F. Vissani, "Spectra of neutrinos from dark matter annihilations", *Nucl.Phys.* **B727** (2005) 99–138, arXiv:hep-ph/0506298 [hep-ph].

[16] O. Mena, S. Palomares-Ruiz, and S. Pascoli, "Reconstructing WIMP properties with neutrino detectors", *Phys.Lett.* **B664** (2008) 92–96, arXiv:0706.3909 [hep-ph].

[17] M. Blennow, J. Edsjö, and T. Ohlsson, "Neutrinos from WIMP annihilations using a full three-flavor Monte Carlo", *JCAP* **0801** (2008) 021, arXiv:0709.3898 [hep-ph].

[18] G. Wikström and J. Edsjö, "Limits on the WIMP-nucleon scattering cross-section from neutrino telescopes", *JCAP* **0904** (2009) 009, arXiv:0903.2986 [astro-ph.CO].

[19] C. Rott, T. Tanaka, and Y. Itow, "Enhanced sensitivity to dark matter self-annihilations in the Sun using neutrino spectral information", *JCAP* **1109** (2011) 029, arXiv:1107.3182 [astro-ph.HE].

[20] C. R. Das, O. Mena, S. Palomares-Ruiz, and S. Pascoli, "Determining the dark matter mass with DeepCore", arXiv:1110.5095 [hep-ph]. To be published in *Phys.Lett.* **B**.

[21] **Super-Kamiokande** Collaboration, K. Bays *et al.*, "Supernova relic neutrino search at Super-Kamiokande", *Phys.Rev.* **D85** (2012) 052007, arXiv:1111.5031 [hep-ex].

[22] K. Bays, *Search for the diffuse supernova neutrino background at Super-Kamiokande*. PhD thesis, University of California, Irvine, 2012.

[23] **Super-Kamiokande** Collaboration, K. Ueno *et al.*, "Search for GUT monopoles at Super-Kamiokande", *Astropart.Phys.* **36** (2012) 131–136, arXiv:1203.0940 [hep-ex].

[24] C. Rott, J. Siegal-Gaskins, and J. F. Beacom, "New sensitivity to solar WIMP annihilation using low-energy neutrinos", arXiv:1208.0827 [astro-ph.HE].

[25] D. Spergel and W. Press, "Effect of hypothetical, weakly interacting, massive particles on energy transport in the solar interior", *Astrophys.J.* **294** (1985) 663–673.

[26] J. Faulkner and R. L. Gilliland, "Weakly interacting, massive particles and the solar neutrino flux", *Astrophys.J.* **299** (1985) 994–1000.

[27] M. Asplund, N. Grevesse, A. J. Sauval, and P. Scott, "The chemical composition of the Sun",

Ann.Rev.Astron.Astrophys. **47** (2009) 481–522, arXiv:0909.0948 [astro-ph.SR].

[28] A. M. Serenelli, W. Haxton, and C. Peña-Garay, "Solar models with accretion. I. Application to the solar abundance problem", *Astrophys.J.* **743** (2011) 24, arXiv:1104.1639 [astro-ph.SR].

[29] M. Nauenberg, "Energy transport and evaporation of weakly interacting particles in the Sun", *Phys.Rev.* **D36** (1987) 1080.

[30] A. Gould and G. Raffelt, "Thermal conduction by massive particles", *Astrophys.J.* **352** (1990) 654.

[31] A. Gould, "Evaporation of wimps with arbitrary cross sections", *Astrophys.J.* **356** (1990) 302–309.

[32] J. R. Ellis and R. Flores, "Realistic predictions for the detection of supersymmetric dark matter", *Nucl.Phys.* **B307** (1988) 883.

[33] J. Engel and P. Vogel, "Spin dependent cross-sections of weakly interacting massive particles on nuclei", *Phys.Rev.* **D40** (1989) 3132–3135.

[34] J. Engel, S. Pittel, and P. Vogel, "Nuclear physics of dark matter detection", *Int.J.Mod.Phys.* **E1** (1992) 1–37.

[35] P. Divari, T. Kosmas, J. Vergados, and L. Skouras, "Shell model calculations for light supersymmetric particle scattering off light nuclei", *Phys.Rev.* **C61** (2000) 054612.

[36] P. Scott, M. Fairbairn, and J. Edsjö, "Dark stars at the galactic centre - the main sequence", *Mon.Not.Roy.Astron.Soc.* **394** (2009) 82, arXiv:0809.1871 [astro-ph].

[37] A. Gould, "WIMP distribution in and evaporation from the Sun", *Astrophys.J.* **321** (1987) 560.

[38] A. Gould, "Resonant enhancements in WIMP capture by the Earth", *Astrophys.J.* **321** (1987) 571.

[39] A. Bottino, G. Fiorentini, N. Fornengo, B. Ricci, S. Scopel, and F. L. Villante, "Does solar physics provide constraints to weakly interacting massive particles?", *Phys.Rev.* **D66** (2002) 053005, arXiv:hep-ph/0206211 [hep-ph].

[40] K. Griest and D. Seckel, "Cosmic asymmetry, neutrinos and the Sun", *Nucl.Phys.* **B283** (1987) 681.

[41] **GEANT4** Collaboration, S. Agostinelli *et al.*, "GEANT4: A simulation toolkit", *Nucl.Instrum.Meth.* **A506** (2003) 250–303.

[42] **GEANT4** Collaboration, J. Allison *et al.*, "GEANT4 developments and applications", *IEEE Trans.Nucl.Sci.* **53** (2006) 270.

[43] T. Sjostrand, S. Mrenna, and P. Z. Skands, "PYTHIA 6.4 physics and manual", *JHEP* **0605** (2006) 026, arXiv:hep-ph/0603175 [hep-ph].

[44] C. Lunardini and A. Y. Smirnov, "Supernova neutrinos: Earth matter effects and neutrino mass spectrum", *Nucl.Phys.* **B616** (2001) 307–348, arXiv:hep-ph/0106149 [hep-ph].

[45] O. L. Peres and A. Y. Smirnov, "Oscillations of very low energy atmospheric neutrinos", *Phys.Rev.* **D79** (2009) 113002, arXiv:0903.5323 [hep-ph].

[46] D. Forero, M. Tortola, and J. Valle, "Global status of neutrino oscillation parameters after Neutrino-2012", *Phys.Rev.* **D86** (2012) 073012, arXiv:1205.4018 [hep-ph].

[47] **Super-Kamiokande** Collaboration, M. Malek *et al.*, "Search for supernova relic neutrinos at Super-Kamiokande", *Phys.Rev.Lett.* **90** (2003) 061101, arXiv:hep-ex/0209028 [hep-ex].

[48] M. Malek, *A search for supernova relic neutrinos.* PhD thesis, State University of New York, Stony Brook, 2003.

[49] S. Palomares-Ruiz and S. Pascoli, "Testing MeV dark matter with neutrino detectors", *Phys.Rev.* **D77** (2008) 025025, arXiv:0710.5420 [astro-ph].

[50] S. Palomares-Ruiz, "Model-independent bound on the dark matter lifetime", *Phys.Lett.* **B665** (2008) 50–53, arXiv:0712.1937 [astro-ph].

[51] A. Strumia and F. Vissani, "Precise quasielastic neutrino/nucleon cross-section", *Phys.Lett.* **B564** (2003) 42–54, arXiv:astro-ph/0302055 [astro-ph].

[52] P. Vogel and J. F. Beacom, "Angular distribution of neutron inverse beta decay, $\bar{\nu}_e + p \to e^+ + n$", *Phys.Rev.* **D60** (1999) 053003, arXiv:hep-ph/9903554 [hep-ph].

[53] R. Smith and E. Moniz, "Neutrino reactions on nuclear targets", *Nucl.Phys.* **B43** (1972) 605.

[54] **Super-Kamiokande** Collaboration, J. Hosaka *et al.*, "Solar neutrino measurements in Super-Kamiokande-I", *Phys.Rev.* **D73** (2006) 112001, arXiv:hep-ex/0508053 [hep-ex].

[55] **Super-Kamiokande** Collaboration, J. Cravens *et al.*, "Solar neutrino measurements in Super-Kamiokande-II", *Phys.Rev.* **D78** (2008) 032002, arXiv:0803.4312 [hep-ex].

[56] **Super-Kamiokande** Collaboration, K. Abe *et al.*, "Solar neutrino results in Super-Kamiokande-III", *Phys.Rev.* **D83** (2011) 052010, arXiv:1010.0118 [hep-ex].

[57] G. Battistoni, A. Ferrari, T. Montaruli, and P. Sala, "The FLUKA atmospheric neutrino flux calculation", *Astropart.Phys.* **19** (2003) 269–290, arXiv:hep-ph/0207035 [hep-ph].

[58] G. Battistoni, A. Ferrari, T. Montaruli, and P. Sala, "The atmospheric neutrino flux below 100-MeV: The FLUKA results", *Astropart.Phys.* **23** (2005) 526–534.

[59] **SIMPLE** Collaboration, M. Felizardo *et al.*, "Final analysis and results of the phase II SIMPLE dark matter search", *Phys.Rev.Lett.* **108** (2012) 201302, arXiv:1106.3014 [astro-ph.CO].

[60] **PICASSO** Collaboration, S. Archambault *et al.*, "Constraints on low-mass WIMP interactions on ^{19}F from PICASSO", *Phys.Lett.* **B711** (2012) 153–161, arXiv:1202.1240 [hep-ex].

[61] **COUPP** Collaboration, E. Behnke *et al.*, "First dark matter search results from a 4-kg CF_3I bubble chamber operated in a deep underground site", *Phys.Rev.* **D86** (2012) 052001, arXiv:1204.3094 [astro-ph.CO].

[62] **Super-Kamiokande** Collaboration, T. Tanaka *et al.*, "An indirect search for WIMPs in the Sun using 3109.6 days of upward-going muons in Super-Kamiokande", *Astrophys.J.* **742** (2011) 78, arXiv:1108.3384 [astro-ph.HE].

[63] R. Kappl and M. W. Winkler, "New limits on dark matter from Super-Kamiokande", *Nucl.Phys.* **B850** (2011) 505–521, arXiv:1104.0679 [hep-ph].

[64] **IceCube** Collaboration, M. Aartsen *et al.*, "Search for dark matter annihilations in the Sun with the 79-string IceCube detector", *Phys.Rev.Lett.* **110** (2013) 131302, arXiv:1212.4097 [astro-ph.HE].

[65] **DAMA/LIBRA** Collaboration, R. Bernabei *et al.*, "First results from DAMA/LIBRA and the combined results with DAMA/NaI", *Eur.Phys.J.* **C56** (2008) 333–355, arXiv:0804.2741 [astro-ph].

[66] **DAMA/LIBRA** Collaboration, R. Bernabei *et al.*, "New results from DAMA/LIBRA", *Eur.Phys.J.* **C67** (2010) 39–49, arXiv:1002.1028 [astro-ph.GA].

[67] C. Savage, G. Gelmini, P. Gondolo, and K. Freese, "Compatibility of DAMA/LIBRA dark matter detection with other searches", *JCAP* **0904** (2009) 010, arXiv:0808.3607 [astro-ph].

[68] C. Savage, G. Gelmini, P. Gondolo, and K. Freese, "XENON10/100 dark matter constraints in comparison with CoGeNT and DAMA: Examining the Leff dependence", *Phys.Rev.* **D83** (2011) 055002, arXiv:1006.0972 [astro-ph.CO].

[69] **CoGeNT** Collaboration, C. Aalseth *et al.*, "Results from a search for light-mass dark matter

with a P-type point contact Germanium detector", *Phys.Rev.Lett.* **106** (2011) 131301, arXiv:1002.4703 [astro-ph.CO].

[70] **CDMS** Collaboration, D. Akerib *et al.*, "A low-threshold analysis of CDMS shallow-site data", *Phys.Rev.* **D82** (2010) 122004, arXiv:1010.4290 [astro-ph.CO].

[71] **XENON10** Collaboration, J. Angle *et al.*, "A search for light dark matter in XENON10 data", *Phys.Rev.Lett.* **107** (2011) 051301, arXiv:1104.3088 [astro-ph.CO].

[72] **XENON100** Collaboration, E. Aprile *et al.*, "Dark matter results from 225 live days of XENON100 data", *Phys.Rev.Lett.* **109** (2012) 181301, arXiv:1207.5988 [astro-ph.CO].

[73] M. Lisanti, L. E. Strigari, J. G. Wacker, and R. H. Wechsler, "The dark matter at the end of the galaxy", *Phys.Rev.* **D83** (2011) 023519, arXiv:1010.4300 [astro-ph.CO].

[74] Y.-Y. Mao, L. E. Strigari, R. H. Wechsler, H.-Y. Wu, and O. Hahn, "Halo-to-halo similarity and scatter in the velocity distribution of dark matter", *Astrophys.J.* **764** (2013) 35, arXiv:1210.2721 [astro-ph.CO].

[75] K. Abe *et al.*, "Letter of intent: The Hyper-Kamiokande experiment — Detector design and physics potential —", arXiv:1109.3262 [hep-ex].